actuators

MDPI

Article

3D Printed Device for Separation of Cells and Particles by Tilted Bulk Acoustic Wave Actuation

Adem Ozcelik

Department of Mechanical Engineering, Aydın Adnan Menderes University, Aydın 09010, Turkey; aozcelik@adu.edu.tr

Abstract: Three-dimensional (3D) printing has been proven to be a reliable manufacturing method for a diverse set of applications in engineering. Simple benchtop tools such as mini centrifuges, automated syringe pumps, and basic-robotic platforms have been successfully printed by basic 3D printers. The field of lab-on-a-chip offers promising functions and convenience for point-of-care diagnostics and rapid disease screening for limited resource settings. In this work, stereolithography (SLA) 3D resin printing is implemented to fabricate a microfluidic device to be used for separation of HeLa cells from smaller polystyrene particles through titled angle standing bulk acoustic wave actuation. The demonstrated device achieved continuous and efficient separation of target cells with over 92% HeLa cell purity and 88% cell recovery rates. Overall, 3D printing is shown to be a viable method for fabrication of microfluidic devices for lab-on-a-chip applications.

Keywords: microfluidics; 3D printing; acoustic separation

Citation: Ozcelik, A. 3D Printed Device for Separation of Cells and Particles by Tilted Bulk Acoustic Wave Actuation. *Actuators* **2022**, *11*, 249. https://doi.org/10.3390/act11090249

Academic Editor: Nicola Pio Belfiore

Received: 3 August 2022
Accepted: 30 August 2022
Published: 31 August 2022

1. Introduction

Separation of heterogenous particle and cell mixtures is an important task for various applications in chemical sciences, biology, and medical fields [1,2]. Especially for cell-based therapies and medical research, isolation of different cell types and removal of undesired particles such as bacteria and debris from cell solutions is critical for diagnostic and therapeutic purposes. Currently, these cell isolation and washing procedures generally rely on expensive and bulky equipment which are not readily available in developing countries. The field of microfluidics present new opportunities with small volumes and miniaturized mechanisms that can enable simple and low-cost tools for biomedical applications for resource-limited environments [3–7].

There are various approaches to separate target particles or cells from a heterogenous solution [8]. A commonly used method is centrifugation of mixed solutions that can separate suspended particles based on their density differences [9]. During this process, high shear forces can be exerted to cells at high gravitational accelerations which can be detrimental to living cells. Furthermore, centrifugation-based methods usually require lengthy and laborious steps which may result in sample contamination. Microfluidic platforms have also been implemented in separation of different types of cells and particles [10]. Microfluidic-based methods can be grouped into two categories as passive and active separation methods [11]. Passive methods include deterministic lateral displacement (DLD), inertial microfluidics, microfiltration, hydrodynamic filtration, and pinch-flow fractionation [12–15]. In filtration-based methods, the major issue is device clogging. Apart from this, most of the passive separation methods lack the sample type dependent dynamic adjustability. For example, DLD-based devices are usually designed for certain sample properties; for different particle size and geometry, different device structures may be required.

Active forces have also been implemented in microfluidic cell separation applications including electrophoresis, dielectrophoresis, magnetophoresis, optical tweezers, and acoustophoresis [10,16–22]. For example, Song et al. applied dielectrophoresis forces in

a continuous flow device to separate human mesenchymal stem cells (hMSCs) and differentiated products [23]. They reported collection efficiencies over 92% and 67% for hMSCs and osteoblasts. Piacentini et al. demonstrated implementation of dielectrophoresis in separation of platelets from blood samples and reported 98.8% platelet purity [24]. Even though dielectrophoresis-based cell separation has been shown to result in high separation efficiencies, this method requires expensive device fabrication steps and specific requirements on sample and liquid medium conductivity. In magnetophoresis-based separation methods, particle separation occurs due to selective attraction to an external magnetic field [25]. Therefore, magnetic labeling is generally required for inherently non-magnetic cells and particles [26]. In acoustic-based methods, particles with different sizes, densities, and mechanical properties can be manipulated through the differential effect of acoustic radiation forces [27–30]. Acoustophoresis-based separation methods have been demonstrated in various cell and particle separation applications [31–35]. For example, Li et al. presented a standing surface acoustic-based approach to separate *Escherichia coli* and human blood cells with 96% cell purity [36]. Acoustophoresis-based methods generally does not require labeling and result in high separation efficiencies, but device preparation in these systems requires expensive central facilities and lengthy fabrication procedures including multiple steps of lithography for fluidic parts, and metal deposition and lift-off for the interdigital transducers in SAW devices. Overall, the existing microfluidic devices for active particle separation rely on cleanroom fabrication facilities which are not available to majority of researchers. Therefore, different approaches to device fabrication for cell separation is needed to enable alternative methods for resource-limited laboratories.

In this work, a three-dimensional (3D) printed microfluidic device is fabricated and applied in separating HeLa cells and polystyrene microparticles by using tilted standing bulk acoustic wave (SBAW) approach. In recent years, 3D printing has been increasingly adopted in device manufacturing, providing a cheap and rapid prototyping option [37–41]. Here, a consumer grade resin printer is implemented to print a transparent fluidic channel, and piezo ceramic transducers are used to assemble an acoustophoretic device. HeLa cells are separated from 1 μm diameter polystyrene particles which are selected to simulate bacteria. The presented low-cost and simple device enabled around 88% cell recovery efficiencies and 92% cell purity which are comparable to the performance of the existing acoustophoretic separation devices that are complex and expensive to fabricate. The demonstrated 3D printed tilted SBAW device shows promising potential in biomedical applications.

2. Materials and Methods

A consumer grade resin 3D printer (Photon S, ANYCUBIC, Shenzhen, China) was used to fabricate the microfluidic device. A clear color 405 nm photocurable resin (Basic clear, ANYCUBIC, Shenzhen, China) was used in the printer. As for the printing parameters, layer height was chosen to be 20 μm, and exposure time, off-time, bottom layer count, and bottom exposure time were selected as 8 s, 1 s, 8, and 60 s, respectively. After printing the device, a thin layer of uncured resin was applied around the device and cured at 405 nm UV light to obtain a better surface finish and higher transparency. Then, polyethylene tubing was inserted into inlets and outlets of the device. Finally, two piezoceramic transducers (SMPL20W15T3R111, Stem, Inc., Pompano Beach, FL, USA) were bonded on the sides of the channel using a fast-curing epoxy (E340, Akfix, Istanbul, Turkey). The microfluidic channel was designed to have a tilted mid-section, as shown in Figure 1. The fluidic channel width and height are 1.5 mm and 0.3 mm, respectively. The tilted section of the micro channel has a length of 16 mm, and before and after this section there is a 2.5 mm straight part. The microfluidic device was designed to have three inlets and two outlets as shown in Figure 1.

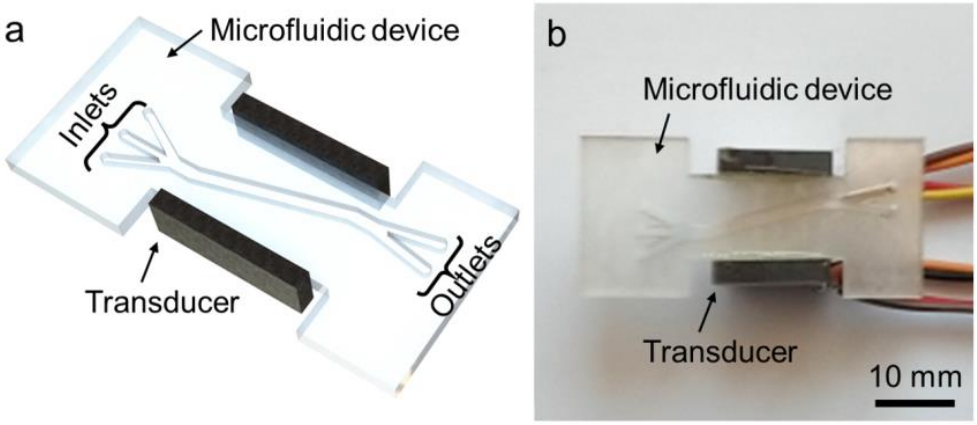

Figure 1. The 3D printed and assembled microfluidic device. (**a**) Schematic depiction of the device geometry. (**b**) Actual picture of the acoustic device.

The experiments were conducted on the sample stage of an inverted optical microscope (OX.2053-PLPH, Euromex, Arnhem, The Netherlands) equipped with 10× and 20× objective lends and a CMOS camera (HD, Euromex, Arnhem, Netherlands). The piezo ceramic transducers were driven at higher harmonics and their working frequency was determined using a vector network analyzer (NanoVNA, Huayang, Guangdong, China). A resonance mode of the transducers that was observed at 10.11 MHz (Figure 2) was implemented in the experiments. A function generator (TBS2104, Tektronix, OR, USA) was used to drive the transducers. A custom-built RF amplifier was used to amplify the driving frequency. Two transducers were driven at the same driving frequency. A programmable syringe pump was employed to infuse the solutions into the device [42]. The experimental setup is shown in Figure 3.

HeLa cells were maintained in DMEM/F12 cell medium with 10% fetal bovine serum (Gibco, Life Technologies, Carlsbad, CA, USA). For the separation experiments, HeLa cells with a concentration of 10^6 cell/mL were suspended in phosphate buffered saline solution and mixed with 1 µm polystyrene particles with approximately 10^7 particles/mL. A standard hemocytometer was used to analyze the cell counts in the experiments. HeLa cell viability was evaluated using Trypan blue staining. For this, HeLa cells were suspended in 1 mL PBS solution added with 0.4% trypan blue. After 3 min incubation, viable (unstained) cells were counted using a hemacytometer.

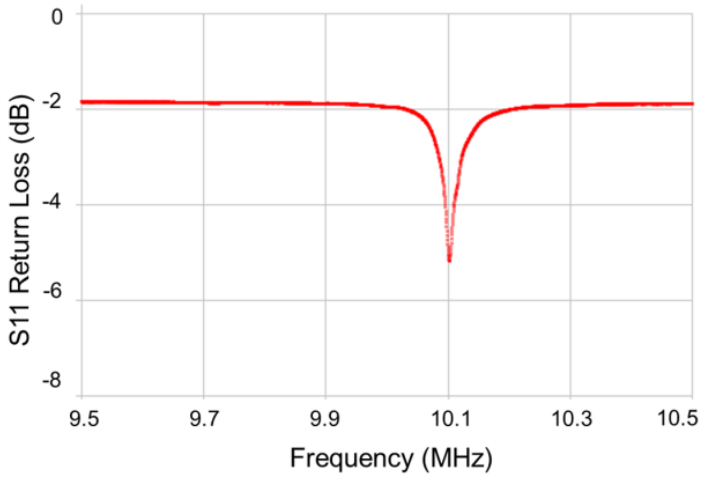

Figure 2. Resonance frequency analysis of the piezo ceramic transducer.

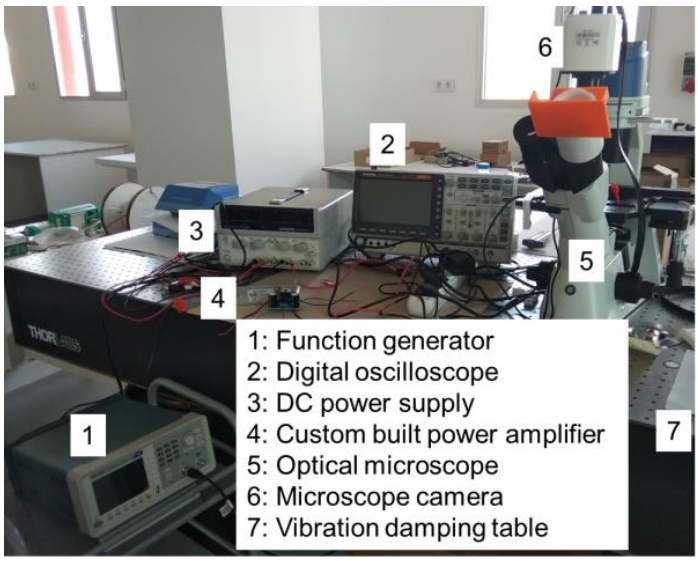

Figure 3. Experimental setup that is used for this study is shown.

3. Results

3.1. Working Mechanism

In the acoustic device, two oppositely positioned transducers are driven at about 10.11 MHz frequency, which can establish a standing bulk acoustic wave field inside the fluidic channel. The standing wave field includes an array of alternating minimum and maximum acoustic pressure regions (nodes). The tilted geometry of the channel result in a 15° angle between the pressure nodes. This angle was selected based on the standing surface acoustic wave literature that implement tilted geometry for cell manipulation. Cells and particles suspended in the fluid near a pressure node experience an acoustic radiation force given by [43]:

$$F_R = -\left(\frac{\pi p_o^2 V_p \beta_f}{2\lambda}\right)\phi(\beta,\rho)\sin(2kx) \quad (1)$$

$$\phi(\beta,\rho) = \frac{5\rho_p - \rho_f}{2\rho_p + \rho_f} - \frac{\beta_p}{\beta_f} \quad (2)$$

here, v_p, β_f, β_p, ρ_f, ρ_p, and p_0 are volume of the particle, compressibility of fluid, compressibility of particle density of fluid, density of particle, and acoustic pressure, respectively. ϕ, x, λ, and k are the acoustic contrast, distance of a particle from node line, wavelength, and wavenumber, respectively. The acoustic contrast factor is an important parameter that determines the direction of the acoustic radiation force (towards pressure node or antinode) based on the relative density of the particle with respect to the fluid. The acoustic radiation force scales with the particle size, density, and compressibility. Thus, a larger particle experiences a bigger force compared to smaller particle.

Another important force that influences the behavior of suspended particles in a fluid flow is Stoke's drag force ($\boldsymbol{F_{St}}$) which depends on the radius of the suspended particles (a_S), dynamic viscosity of the fluid (μ), and the relative velocity of the particle with respect to the velocity of the fluid. For particles with smaller sizes, $\boldsymbol{F_{St}}$ dominates over the acoustic radiation force [44]. Stoke's drag force is given by:

$$\boldsymbol{F}_{St} = 6\,\pi\mu a_S u_S \quad (3)$$

In Figure 4a, cell and particle separation is schematically illustrated. In this device, cell and particle suspension in infused from the center inlet and hydrodynamically focused before entering the acoustic field. In the laminar flow, cells and particles preserve their relative position inside the channel. In the standing acoustic field, the periodic linear

pressure field that are aligned with a tilt angle to the flow direction forces suspended inclusions to move along the minimum pressure lines. In this process, the acoustic radiation force pushes cells and particles to the pressure nodes, but larger cells experience a bigger force compared to the particles. Therefore, cells tend to follow the pressure node lines rather than the flow streamline and become separated from the smaller particles. The scaling of the acoustic radiation force for 10 µm, 7 µm, 5 µm, and 1 µm polystyrene particles is given in Figure 4b. In this calculation, the fluid medium is considered as water, acoustic pressure is assumed to be 0.2 MPa, the acoustic wavelength is set to be 150 µm, compressibility of the particles and the fluid are 4.58×10^{-10} Pa^{-1} and 2.46×10^{-10} Pa^{-1}, and density of the particles and the fluid are 1050 kg m^{-3} and 1000 kg m^{-3}, respectively [17,45,46]. From Equations (1) and (2), it is evident that 10 µm diameter particle will experience a much larger acoustic radiation force compared to smaller particles. It is also evident that particles with higher densities will result in a larger force. Because HeLa cells (1040 kg m^{-3}) and polystyrene particles (1050 kg m^{-3}) have very similar densities, their volume differences will have a rather significant effect on the scale of the acoustic radiation forces.

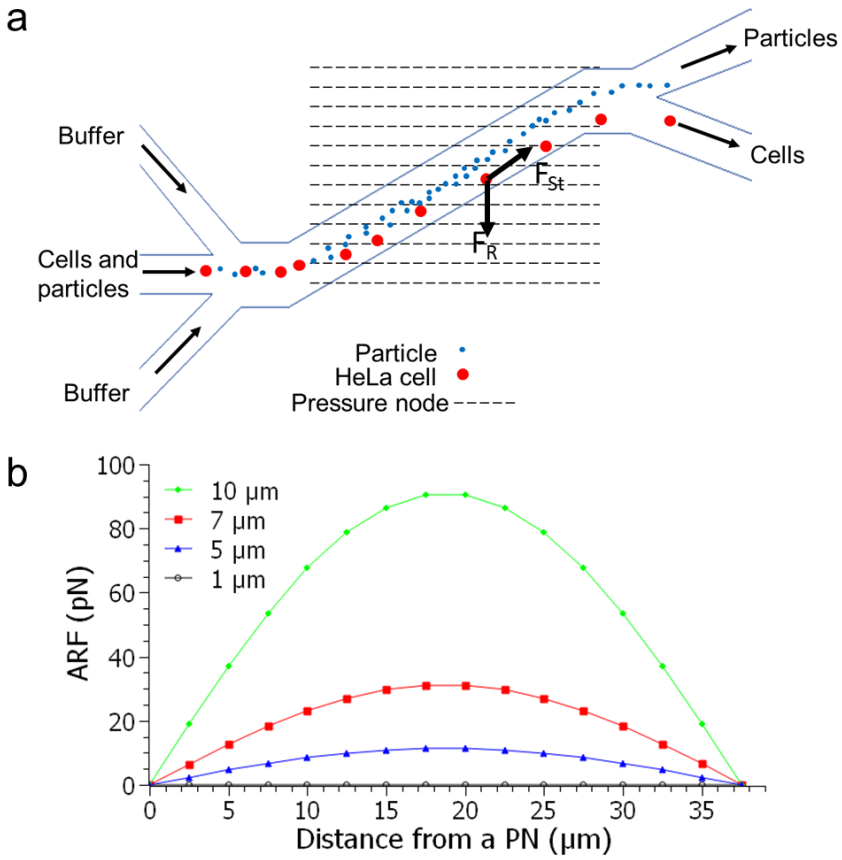

Figure 4. Working principle of the acoustic device. (**a**) A schematic depiction of the acoustic device geometry and acoustic pressure nodes. F_R: Acoustic radiation force, F_{St}: Stoke's drag force. (**b**) Plot of the acoustic radiation force for different size polystyrene microparticles. PN: pressure node. ARF: Acoustic radiation force.

3.2. Cell and Particle Separation

HeLa cell and 1 µm polystyrene particle mixture was injected from the center inlet of the device and focused with the PBS buffer flows. Lower and upper inlet flow rates were 20 and 30 µL/min, and the sample inlet flow rate was 10 µL/min. This way all the suspended cells and particles were directed to the upper outlet of the device when the acoustic field was off (Figure 5a). When the standing acoustic wave field was established, HeLa cells started following the pressure nodes and deflected from the mid-flow streamlines as sown

in Figure 5b. On the other hand, 1 µm diameter polystyrene particles were not affected by the acoustic radiation force and kept following the laminar flow.

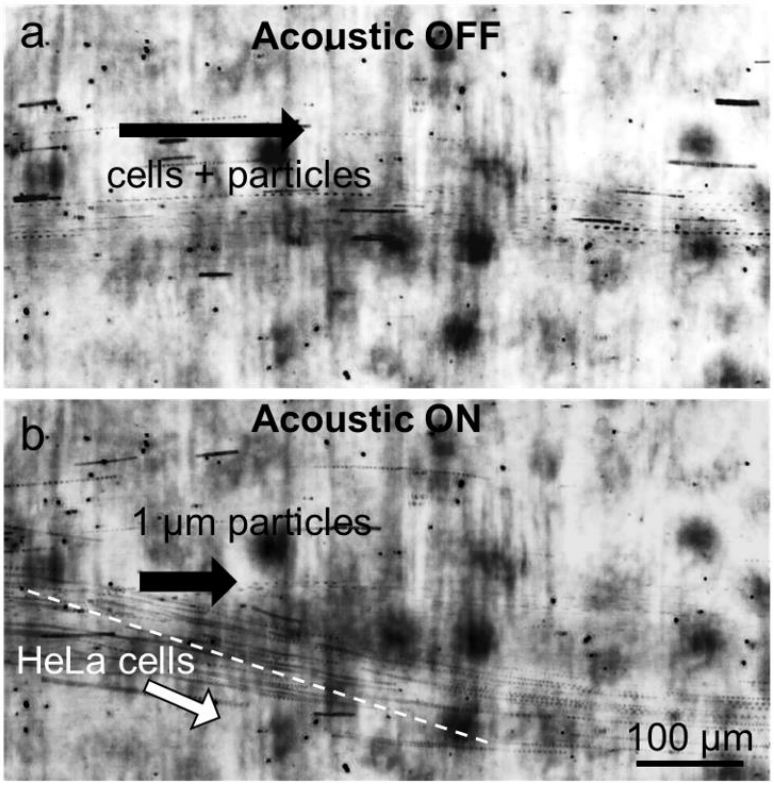

Figure 5. Separation of HeLa cells and polystyrene particles is shown by stacked images. (**a**) When the acoustic field is turned off, the mixture of the particles and cells flow together. (**b**) In the standing acoustic wave field, HeLa cells mostly follow the pressure nodes and separated from the smaller polystyrene particles.

The deflection of the HeLa cells needs to be high enough to separate them from the particles and cell debris and push them to the lower outlet. For this, increasing power amplitudes were applied and for each case number of HeLa cells recovered from the original solution was characterized as shown in Figure 6. Starting from 20 V_{PP}, the applied voltage was increased up to 60 V_{PP} which was the highest voltage provided by the amplifier circuit. At the highest voltage, over 88% HeLa cell recovery was obtained at around 92% cell purity. Cell recovery rate is calculated by the ratio of the number of the sorted target cells and the number of the target cells available for separation. Cell purity is defined as the ratio of the number of the target cells isolated and the total number of the cells and particles isolated. Cell viability is defined as the ratio between the difference of total number of cells–stained cells and the total number of cells. Here, the stained cells are the dead ones that intake the staining dye. The viability of the HeLa cells was also characterized after they are acoustically being separated from the particles. HeLa cell viability values for increasingly higher applied voltages are shown in Figure 7. At lower voltage amplitudes, the viability of the HeLa cells was found to be over 95%. As the voltage was increased, the viability was dropped to about 90% at 60 V_{PP}.

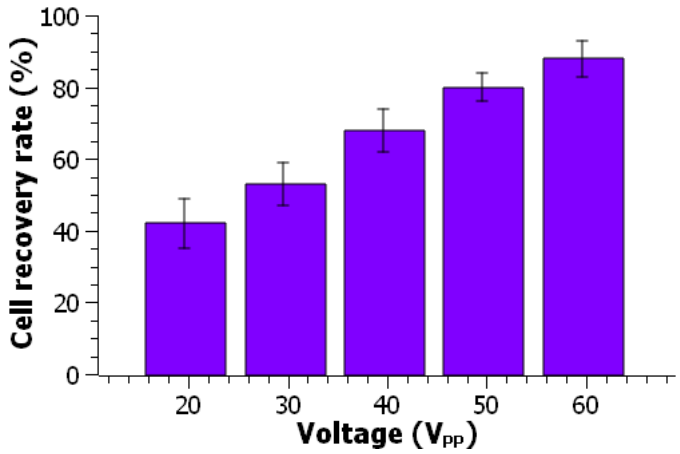

Figure 6. Characterization of HeLa cell recovery efficiency as a function of the applied voltage. Error bars are standard deviation of 5 measurements.

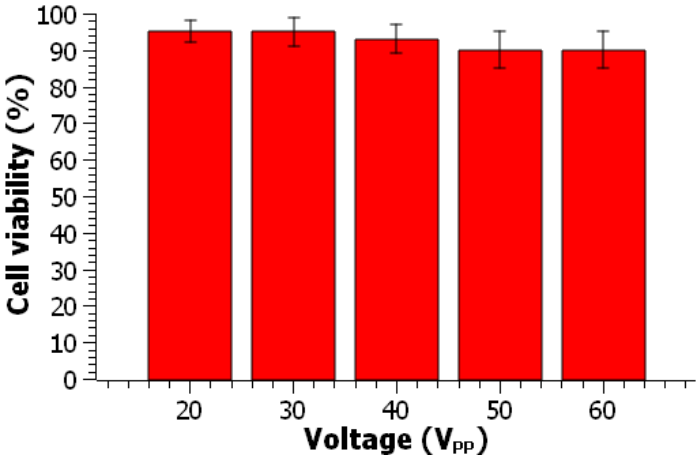

Figure 7. Characterization of HeLa cell viability of acoustic separation. Error bars are standard deviation of 5 measurements.

4. Discussion

While lab-on-a-chip platforms can provide sample preparation, disease diagnostics, and bioanalysis in a small chip, the fabrication of lab-on-chip devices is still a challenging and expensive task in low-resource settings. In this work, stereolithography (SLA) 3D printing provided a simple and rapid approach for fabricating a microfluidic device to separate HeLa cells from the stream of polystyrene particles using tilted angle standing bulk acoustic waves. Overall, the device was printed with decent surface quality, but a thin layer of uncured resin application and subsequent curing greatly enhanced the surface roughness and improved the optical clarity of the device in the channel region. It was observed that the printing resolution of the device can affect the flow behavior inside the channel due to the undesired imperfections within device. These imperfections can also influence the cell separation performance negatively by unwanted flow perturbations. This device fabrication method is very convenient for researchers with limited budgets and infrastructure including cleanroom lithography facilities. Even though the printing resolution of most of the SLA printers is not as low as the resolutions that can be acquired through optical lithography, 3D printing can still be applied in numerous microfluidic applications that do not need minimum feature sizes lower than roughly 50 μm. With the advancement of the SLA printers, the resolution of these printers could be improved in the future.

The presented acoustic device demonstrated over 90% efficient HeLa cells separation efficiency. In Figure 5, the recovery efficiency of HeLa cell is shown to increase with the increasing applied power. At 20 V_{PP}, the cell recovery efficiency is about 40%, and at 60 V_{PP}, cell recovery goes up to 88%. This is meaningful because the acoustic radiation force scales with the acoustic pressure. As the power applied to the transducers is increased, the acoustic radiation force also increases. A larger acoustic radiation force is more effective to deviate the HeLa cells from their laminar flow and push them to the lower collection outlet. On the other hand, 1 µm polystyrene particles stay in the center flow because the acoustic radiation force exerted on these particles is about 1000 times smaller due their smaller volumes. The output of the power amplifier used in this work is limited to 60 V_{PP}. With larger power amplitudes, it could be possible to attain better recovery efficiencies. At the current device operation parameters, the HeLa cells showed over 90% viability rate, which is comparable to the reported literature [47]. If higher powers will be applied to improve the device performance, an active cooling strategy could be needed to prevent device overheating which can negatively affect the cell viability. In the current acoustic system, 60 V_{PP} applied voltage results in 88% cell recovery rate and about 90% cell viability which is acceptable for basic cell separation studies. Here, the most important parameters are cell recovery and cell purity, which can be critical to keep important target cells for therapeutic applications. If the cell viability is over 90 percent, these separation yields can be considered significant for general purposes.

5. Conclusions

Herein, SLA printing is shown to be a viable solution for fabricating microfluidic devices for acoustofluidic applications. The acoustic device shown here is capable of separating HeLa cells from smaller particles with decent cell purity (92%) and recovery (88%) rates under the applied voltage of 60 Vpp and driving frequency of 10.11 MHz. On-chip cell washing and separation from bacteria are useful and desired capabilities for cell-based therapies, rapid diagnostics, and sample preparation. Implementation of 3D printed microfluidic devices in biomedical research is promising for widespread adaptation of low-cost and open-sourced tools for the researchers in low-income countries.

Funding: This work was supported by the Aydın Adnan Menderes University Research Fund (BAP), Project Number: MF-20002.

Institutional Review Board Statement: Not applicable.

Informed Consent Statement: Not applicable.

Data Availability Statement: Not applicable.

Acknowledgments: We thank Zeynep Aslan and Fatih Akkoyun for their suggestions and recommendations.

Conflicts of Interest: The author declares no conflict of interest.

References

1. Yousuff, C.; Ho, E.; Hussain, K.I.; Hamid, N. Microfluidic Platform for Cell Isolation and Manipulation Based on Cell Properties. *Micromachines* **2017**, *8*, 15. [CrossRef]
2. Catarino, S.O.; Rodrigues, R.O.; Pinho, D.; Miranda, J.M.; Minas, G.; Lima, R. Blood Cells Separation and Sorting Techniques of Passive Microfluidic Devices: From Fabrication to Applications. *Micromachines* **2019**, *10*, 593. [CrossRef] [PubMed]
3. Akkoyun, F.; Özçelik, A. A Battery-Powered Fluid Manipulation System Actuated by Mechanical Vibrations. *Actuators* **2022**, *11*, 116. [CrossRef]
4. Ozcelik, A.; Rich, J.; Huang, T.J. Fundamentals and Applications of Acoustics in Microfluidics. In *Multidisciplinary Microfluidic and Nanofluidic Lab-on-a-Chip*; Elsevier: Amsterdam, The Netherlands, 2022; pp. 297–321.
5. Wu, Z.; Cai, H.; Ao, Z.; Nunez, A.; Liu, H.; Bondesson, M.; Guo, S.; Guo, F. A Digital Acoustofluidic Pump Powered by Localized Fluid-Substrate Interactions. *Anal. Chem.* **2019**, *91*, 7097–7103. [CrossRef] [PubMed]
6. Ao, Z.; Cai, H.; Wu, Z.; Song, S.; Karahan, H.; Kim, B.; Lu, H.-C.; Kim, J.; Mackie, K.; Guo, F. Tubular Human Brain Organoids to Model Microglia-Mediated Neuroinflammation. *Lab Chip* **2021**, *21*, 2751–2762. [CrossRef] [PubMed]

7. Ao, Z.; Cai, H.; Wu, Z.; Krzesniak, J.; Tian, C.; Lai, Y.Y.; Mackie, K.; Guo, F. Human Spinal Organoid-on-a-Chip to Model Nociceptive Circuitry for Pain Therapeutics Discovery. *Anal. Chem.* **2022**, *94*, 1365–1372. [CrossRef]
8. Radisic, M.; Iyer, R.K.; Murthy, S.K. Micro- and Nanotechnology in Cell Separation. *Int. J. Nanomed.* **2006**, *1*, 3–14. [CrossRef]
9. Linares, R.; Tan, S.; Gounou, C.; Arraud, N.; Brisson, A.R. High-Speed Centrifugation Induces Aggregation of Extracellular Vesicles. *J. Extracell. Vesicles* **2015**, *4*, 29509. [CrossRef] [PubMed]
10. Nasiri, R.; Shamloo, A.; Ahadian, S.; Amirifar, L.; Akbari, J.; Goudie, M.J.; Lee, K.; Ashammakhi, N.; Dokmeci, M.R.; Di Carlo, D.; et al. Microfluidic-Based Approaches in Targeted Cell/Particle Separation Based on Physical Properties: Fundamentals and Applications. *Small* **2020**, *16*, 2000171. [CrossRef]
11. Shiri, F.; Feng, H.; Gale, B.K. Passive and Active Microfluidic Separation Methods. In *Particle Separation Techniques*; Elsevier: Amsterdam, The Netherlands, 2022; pp. 449–484.
12. Zhao, Q.; Yuan, D.; Zhang, J.; Li, W. A Review of Secondary Flow in Inertial Microfluidics. *Micromachines* **2020**, *11*, 461. [CrossRef]
13. Hawkins, B.G.; Lai, N.; Clague, D.S. High-Sensitivity in Dielectrophoresis Separations. *Micromachines* **2020**, *11*, 391. [CrossRef]
14. Volpe, A.; Gaudiuso, C.; Ancona, A. Sorting of Particles Using Inertial Focusing and Laminar Vortex Technology: A Review. *Micromachines* **2019**, *10*, 594. [CrossRef] [PubMed]
15. Ho, B.; Beech, J.; Tegenfeldt, J. Cell Sorting Using Electrokinetic Deterministic Lateral Displacement. *Micromachines* **2020**, *12*, 30. [CrossRef] [PubMed]
16. Wu, M.; Huang, P.; Zhang, R.; Mao, Z.; Chen, C.; Kemeny, G.; Li, P.; Lee, A.V.; Gyanchandani, R.; Armstrong, A.J.; et al. Circulating Tumor Cell Phenotyping via High-Throughput Acoustic Separation. *Small* **2018**, *14*, 1801131. [CrossRef]
17. Guldiken, R.; Jo, M.C.; Gallant, N.D.; Demirci, U.; Zhe, J. Sheathless Size-Based Acoustic Particle Separation. *Sensors* **2012**, *12*, 905–922. [CrossRef]
18. Witek, M.A.; Freed, I.M.; Soper, S.A. Cell Separations and Sorting. *Anal. Chem.* **2020**, *92*, 105–131. [CrossRef]
19. Xuan, X. Recent Advances in Continuous-Flow Particle Manipulations Using Magnetic Fluids. *Micromachines* **2019**, *10*, 744. [CrossRef]
20. Song, J.; Song, M.; Kang, T.; Kim, D.; Lee, L.P. Label-Free Density Difference Amplification-Based Cell Sorting. *Biomicrofluidics* **2014**, *8*, 064108. [CrossRef]
21. Wu, Z.; Hjort, K. Microfluidic Hydrodynamic Cell Separation: A Review. *Micro Nanosyst.* **2009**, *1*, 181–192. [CrossRef]
22. Bhagat, A.A.S.; Bow, H.; Hou, H.W.; Tan, S.J.; Han, J.; Lim, C.T. Microfluidics for Cell Separation. *Med. Biol. Eng. Comput.* **2010**, *48*, 999–1014. [CrossRef]
23. Song, H.; Rosano, J.M.; Wang, Y.; Garson, C.J.; Prabhakarpandian, B.; Pant, K.; Klarmann, G.J.; Perantoni, A.; Alvarez, L.M.; Lai, E. Continuous-Flow Sorting of Stem Cells and Differentiation Products Based on Dielectrophoresis. *Lab A Chip* **2015**, *15*, 1320–1328. [CrossRef] [PubMed]
24. Piacentini, N.; Mernier, G.; Tornay, R.; Renaud, P. Separation of Platelets from Other Blood Cells in Continuous-Flow by Dielectrophoresis Field-Flow-Fractionation. *Biomicrofluidics* **2011**, *5*, 034122. [CrossRef] [PubMed]
25. Hejazian, M.; Li, W.; Nguyen, N.-T. Lab on a Chip for Continuous-Flow Magnetic Cell Separation. *Lab A Chip* **2015**, *15*, 959–970. [CrossRef] [PubMed]
26. Modak, N.; Datta, A.; Ganguly, R. Cell Separation in a Microfluidic Channel Using Magnetic Microspheres. *Microfluid. Nanofluid.* **2009**, *6*, 647–660. [CrossRef]
27. Yeo, L.Y.; Friend, J.R. Ultrafast Microfluidics Using Surface Acoustic Waves. *Biomicrofluidics* **2009**, *3*, 012002. [CrossRef]
28. Yeo, L.Y.; Friend, J.R. Surface Acoustic Wave Microfluidics. *Annu. Rev. Fluid Mech.* **2014**, *46*, 379–406. [CrossRef]
29. Cai, H.; Ao, Z.; Hu, L.; Moon, Y.; Wu, Z.; Lu, H.-C.; Kim, J.; Guo, F. Acoustofluidic Assembly of 3D Neurospheroids to Model Alzheimer's Disease. *Analyst* **2020**, *145*, 6243–6253. [CrossRef]
30. Ao, Z.; Cai, H.; Wu, Z.; Ott, J.; Wang, H.; Mackie, K.; Guo, F. Controllable Fusion of Human Brain Organoids Using Acoustofluidics. *Lab A Chip* **2021**, *21*, 688–699. [CrossRef]
31. Destgeer, G.; Lee, K.H.; Jung, J.H.; Alazzam, A.; Sung, H.J. Continuous Separation of Particles in a PDMS Microfluidic Channel via Travelling Surface Acoustic Waves (TSAW). *Lab A Chip* **2013**, *13*, 4210–4216. [CrossRef]
32. Destgeer, G.; Ha, B.H.; Jung, J.H.; Sung, H.J. Submicron Separation of Microspheres via Travelling Surface Acoustic Waves. *Lab A Chip* **2014**, *14*, 4665–4672. [CrossRef]
33. Olofsson, K.; Hammarström, B.; Wiklund, M. Acoustic Separation of Living and Dead Cells Using High Density Medium. *Lab A Chip* **2020**, *20*, 1981–1990. [CrossRef] [PubMed]
34. Collins, D.J.; Ma, Z.; Ai, Y. Highly Localized Acoustic Streaming and Size-Selective Submicrometer Particle Concentration Using High Frequency Microscale Focused Acoustic Fields. *Anal. Chem.* **2016**, *88*, 5513–5522. [CrossRef]
35. Gao, Y.; Wu, M.; Lin, Y.; Xu, J. Acoustic Microfluidic Separation Techniques and Bioapplications: A Review. *Micromachines* **2020**, *11*, 921. [CrossRef] [PubMed]
36. Li, S.; Ma, F.; Bachman, H.; Cameron, C.E.; Zeng, X.; Huang, T.J. Acoustofluidic Bacteria Separation. *J. Micromech. Microeng.* **2017**, *27*, 015031. [CrossRef]
37. Li, J.; Wu, S.; Zhang, W.; Ma, K.; Jin, G. 3D Printing of Silicone Elastomers for Soft Actuators. *Actuators* **2022**, *11*, 200. [CrossRef]
38. Akkoyun, F.; Gucluer, S.; Ozcelik, A. Potential of the Acoustic Micromanipulation Technologies for Biomedical Research. *Biomicrofluidics* **2021**, *15*, 061301. [CrossRef]
39. Ozcelik, A.; Aslan, Z. A Practical Microfluidic Pump Enabled by Acoustofluidics and 3D Printing. *Microfluid. Nanofluid.* **2021**, *25*, 5. [CrossRef]

40. Akkoyun, F. Inexpensive Multispectral Imaging Device. *Instrum. Sci. Technol.* **2022**, *50*, 543–559. [CrossRef]
41. Akkoyun, F. A Real-Time Machine Vision System for Grading Quartz Mineral. *J. Test. Eval.* **2022**, *50*, 20210758. [CrossRef]
42. Akkoyun, F.; Ozcelik, A. A Simple Approach for Controlling an Open-Source Syringe Pump. *Eur. Mech. Sci.* **2020**, *4*, 166–170. [CrossRef]
43. Yosioka, K.; Kawasima, Y. Acoustic Radiation Pressure on a Compressible Sphere. *Acustica* **1955**, *5*, 167–173.
44. Ahmed, D.; Ozcelik, A.; Bojanala, N.; Nama, N.; Upadhyay, A.; Chen, Y.; Hanna-Rose, W.; Huang, T.J. Rotational Manipulation of Single Cells and Organisms Using Acoustic Waves. *Nat. Commun.* **2016**, *7*, 11085. [CrossRef] [PubMed]
45. Ozcelik, A.; Huang, T.J. Acoustic Tweezers for Single-Cell Manipulation. In *Handbook of Single Cell Technologies*; Springer: Singapore, 2020; pp. 1–27.
46. Reichert, P.; Deshmukh, D.; Lebovitz, L.; Dual, J. Thin Film Piezoelectrics for Bulk Acoustic Wave (BAW) Acoustophoresis. *Lab Chip* **2018**, *18*, 3655–3667. [CrossRef]
47. Levario-Diaz, V.; Bhaskar, P.; Carmen Galan, M.; Barnes, A.C. Effect of Acoustic Standing Waves on Cellular Viability and Metabolic Activity. *Sci. Rep.* **2020**, *10*, 8493. [CrossRef]